Journal of ELECTRONIC MATERIALS, Vol. 49, No. 1, 2020
https://doi.org/10.1007/s11664-019-07783-6

Enhanced Charge Transport and Corrosion Protection Properties of Polyaniline–Carbon Nanotube Composite Coatings on Mild Steel

T. RAJYALAKSHMI,[1] APSAR PASHA,[2,7] SYED KHASIM,[3,4] MOHANA LAKSHMI,[4] M.V. MURUGENDRAPPA,[5] and NACER BADI[3,6]

1.—Department of Physics, PES University, EC Campus, Bengaluru 560100, India. 2.—Department of Physics, Ghousia College of Engineering, Ramanagaram, Karnataka State 562159, India. 3.—Renewable Energy Laboratory, Nanotechnology Research Unit, Faculty of Science, University of Tabuk, Tabuk 71491, Kingdom of Saudi Arabia. 4.—Department of Physics, PES University, Electronic City Campus, Bengaluru 560100, India. 5.—Center of Excellence in Advanced Materials Research, BMS College of Engineering, Bengaluru 560019, India. 6.—Center for Advanced Materials, University of Houston, Houston, USA. 7.—e-mail: apsarpasha1982@gmail.com

We report on the synthesis and characterization of carbon nanotube (CNT)-doped polyaniline (PANI) composites for enhanced corrosion protection of steel with improved electrical properties. PANI–CNT nanocomposites were prepared through in situ polymerization of aniline in the presence of CNTs. Synthesized nanocomposites were characterized by several analytical methods such as Fourier transform infrared spectroscopy, x-ray diffraction, micro-Raman spectroscopy, and scanning electron microscopy in order to understand the structural, morphological, and molecular aspects of the composites. The doping of CNTs in PANI matrix drastically enhanced the alternating current/direct current (AC/DC) conductivities as well as the dielectric attributes and impedance spectroscopy of the composites. The anticorrosion studies of the prepared composites were performed by using open-circuit potential analysis and potentiodynamic measurements. Compared to stainless steel, PANI–CNT nanocomposites demonstrated excellent anticorrosion behavior. The obtained results showed that 25 wt.% of CNT-doped PANI composite exhibits excellent anticorrosion properties due to electron transmission and passive catalysis.

Key words: Polyaniline, carbon nanotubes, PANI–CNTs, anticorrosion, nanocomposites, electrical conductivity

INTRODUCTION

Polyaniline (PANI) is one of the top resources amongst the family of conducting polymers because of its excellent conductivity, enhanced chemical and thermal stability, low-cost synthesis, and ease of processing for device fabrication. The extended π–π conjugation present along the polymeric backbone accounts for the high conductivity of PANI. Such materials are of high interest and form the building blocks for advanced high-performance-based polymer nanocomposites, exclusively with respect to improved electrical conductivity and thermal and chemical stability.[1–3] The synthesis process of CNT-doped polymer composites was first reported by Ajayan et al.[4] Ever since, there has been an increased number of extensive efforts in combining CNTs with various polymers for improved electrical and mechanical properties.

Generally, carbon exists in many allotropic forms like diamond, coal, graphite, fullerenes, and nanotubes. Among all those allotropic forms, CNTs are tiny tubular structures with length up to 1 mm and

(Received June 15, 2019; accepted October 29, 2019; published online November 12, 2019)

diameter around 0.3–2.6 nm. It is its structure which makes it unique among all other allotropic forms. In particular, the helical arrangement of the honeycomb lattice makes CNTs behave both like metal as well as a semiconductor, and an increased width leads to decrease in the bandgap. The CNTs are of great research interest due to their exquisite thermal stability. Their unique mechanical, thermal, and electrical properties have garnered attention for developing several types of multifunctional composite materials.[5,6] For a few decades now, CNT-doped polymer nanocomposites have been extensively studied due to their remarkable role in areas of both basic and applied sciences.[7,8] Studies have revealed that the doping of CNTs in any host polymer leads to enhancement in electrical conductivity and also improvement in electrochemical and mechanical properties. Generally, the composites prepared by doping of the CNTs in polymer were found to have potential usage in photovoltaic cells,[9] high-capacity batteries, rust proofing, night vision cameras, and flexible electronics. The most effective method to produce dispersals includes ultra-sonication of CNTs in the presence of a polymer which makes it reside on the nanotube surface through non-covalent interactions resulting in stable dispersion of CNTs within the polymer.[10] This method not only enables higher concentration of doping of CNTs in polymer but also results in improved electrical and anticorrosion properties without degrading the properties that chemical modification usually does with CNTs.[11,12] CNT-doped PANI nanocomposites find numerous applications in gas and humidity sensors due to their unique property of reacting with analyte gases,[13,14] as bio-sensing materials,[15] super capacitors,[16] solar cells,[17] fuel cells,[18] and in corrosion protection. Among all the available methods of synthesis for PANI, the most useful method is in situ polymerization. This method enables the filler CNTs to affix on the host PANI matrix effectively, which leads to improved interface amid CNTs and PANI. The incorporation of CNTs as a filler in PANI improves the conductivity of PANI–CNT nanocomposite as CNTs are highly conductive in nature as compared to PANI. CNTs act as conducting networks amid the conducting paths of PANI, resulting in improved conductivity after doping.

The influence of different concentrations of functionalized multi-walled CNTs on the conductivity of PANI–CNT nanocomposites were studied in the present work. For low concentrations of CNTs, PANI predominantly determines the nanocomposite's conductivity. As the weight percentage of CNTs was gradually increased, the conductivity of PANI-based nanocomposite was found to increase.[19–21] An optimal amount of filler loaded into the polymer matrix results in the creation of percolation paths and, consequently, charge transportation occurs throughout the nanocomposite. For a particular concentration which forms the percolation threshold, the conductivity values measured were comparatively the highest. This may be due to the good dispersion of covalently functionalized CNTs which enables a grafting surface. Currently, there is an increased demand for mild steel in both industry and for domestic purposes. Metallic structures need a suitable anticorrosive coating to protect the metal against corrosion; hence, we have selected steel substrate in our present study. In general, a polymer can be applied on steel structures to protect it against corrosion under different environmental conditions such as acidic, alkaline, and neutral conditions.[22–24] PANI alone degrades at a much faster rate in harsh environments and, hence, anticorrosion coatings using PANI are prepared in the form of nanocomposites involving suitable fillers such as CNTs. These smart coatings of PANI–CNT nanocomposites prepared with a suitable resin (binder) provide stability to a polymer backbone against harsh environments and serve as an excellent anticorrosion coating.[25,26]

In this work, we report on a simple method of preparation of CNT-doped PANI nanocomposites with improved properties. An attempt was made to improve the conductivity, dielectric attributes, and corrosion passivation on mild steel. Furthermore, the prepared composites were characterized by scanning electron microscopy (SEM), Fourier transform infrared (FTIR), x-ray diffraction (XRD), and Raman techniques. The temperature-dependent conductivity, frequency-dependent conductivity, and dielectric properties were studied using a laboratory-made setup connected to an impedance analyzer. The CNT-doped PANI thin films were prepared by dip-coating method on steel substrate to test the possible applications toward improved anticorrosion.

EXPERIMENTAL DETAILS

The research-grade chemicals used such as the monomer aniline, ammonium persulfate (APS), hydrochloric acid (HCl), *N*-methyl-2-pyrrolidone (NMP), CNTs, and silver paste were purchased from Sigma Aldrich with 99.98% purity. The tested mild steel substrates (316L) are composed of C (0.02%), P (0.023%), Si (0.04%), Ni (0.017), Mn (0.37%), and Mo (0.02%).

Synthesis of PANI

PANI was prepared by in situ chemical oxidative polymerization technique. The reaction was carried out in a flask containing 1 M solution of aniline and 1 M HCl dissolved in distilled water to obtain aniline hydrochloride. To this solution, 100 mL of 0.1 M APS was added dropwise along with stirring for about 3 h to initiate polymerization. The experiment was performed in a temperature range of 0–5°C. The reacted product was left in an ice bath overnight, and the next day, the solution was

filtered, and PANI precipitate collected was subjected to washings with deionized water and then dried.[27]

Synthesis of CNT-Doped PANI Composites

Composites of PANI doped with CNTs were also prepared by in situ polymerization method. For this, CNTs were added to the solution of aniline hydrochloride, and the mixture was continuously stirred for 30 min to produce a homogenous dispersion of CNTs in aniline hydrochloride solution. Further 0.1 M APS, which acts as an oxidant, was added dropwise slowly with continuous stirring for 3 h while maintaining the temperature at 0–5°C for polymerization of aniline. The next day, the solution was filtered, and the precipitate collected was washed with deionized water and finally dried in an oven for 24 h to achieve a constant weight. Following this procedure, CNT-doped PANI nanocomposites with various weight percentages of CNTs (5 wt.%, 10 wt.%, 15 wt.%, 20 wt.%, and 25 wt.%) in PANI were prepared.

Synthesis of CNT-Doped PANI Thin films

PANI (0.3 g) was dissolved in 5 mL of tetraethylenepentamine (TEPA) under magnetic stirring at room temperature for 1 day for homogenous dispersion of PANI in TEPA. Later, the solution was filtered by using Whatman filter paper of pore size 0.5 μm. Also, CNTs (0.4 g) were mixed with *N*-methyl-2-pyrrolidone (NMP, 10 mL) solvent, and the solution was sonicated for 2 h to produce uniform dispersal of CNTs in NMP. After the sonication process, the solution was filtered using Whatman filter paper of pore size 0.5 μm to obtain a pure solution of CNTs. During the process, polyvinyl butyral (PVB, 5 g) was dissolved in methanol (50 mL) and was kept for 5 h of stirring and then sonicated for 2 h to achieve a homogenous solution of CNTs. Then, pure PANI solution and PANI solution doped with different composition of CNTs (5 wt.%, 10 wt.%, 15 wt.%, 20 wt.%, and 25 wt.%) solution was made into a slurry in methanol and added to PVB solution. This dispersion was sonicated for 12 h to obtain uniform distribution of PANI–CNTs. The stainless-steel substrates were polished with emery paper, washed with acetone, and were finally dried. Thin films of pure PANI and PANI doped with CNTs were prepared by dip-coating method on stainless-steel substrates by using a dip-coating unit (model no.: HO-TH-02) for 50 s. The prepared thin films of pure PANI and CNT-doped PANI were annealed in a hot oven at 60°C for 5 h to remove the moisture absorbed in the prepared thin films.

Characterization Details

The surface morphology and structural analysis of PANI and CNT-doped PANI nanocomposites were characterized by different techniques like SEM, FTIR, XRD, and Raman spectroscopy. The surface morphology of PANI and PANI–CNT nanocomposites were investigated using a TESCAN VEGA3 scanning electron microscope. FTIR spectra were recorded using a Perkin Elmer spectrometer in KBr medium by preparing a transparent pellet. Raman spectroscopy was studied employing a LabRAM HR (UV) system, which gives a high spectroscopic resolution with a 325-nm laser using a charge coupled device (CCD) detector. Structural identification was carried out using an XPERT-3 X-ray diffractometer with Cu$K\alpha$ radiation of 1.54060 Å, and the diffractograms were scanned in the range of 10°–80° with a scan rate of 0.03° per second.

The temperature-dependent electrical conductivity (DC) of PANI and CNT-doped PANI composites pressed into the form of pellets was studied using a laboratory-made setup comprising a Keithley 2182A nano-voltmeter and Keithley 6221 DC and AC current source. The frequency-dependent electrical conductivity (AC) measurements were carried out at ambient temperature by four-probe method utilizing a Wayne Kerr 6500B precision impedance analyzer. The dielectric properties of the samples were also studied using the same frequency analyzer in the frequency range of 100 Hz–5 MHz. The oxygen gas permeability of PANI and PANI–CNT nanocomposites were investigated using a Yanaco GTR-31 gas permeability analyzer (GPA). The oxygen transmission rate and the oxygen permeability of the samples were estimated by gas chromatography technique.

RESULTS AND DISCUSSIONS

Scanning Electron Microscope

The surface morphology of pure PANI and PANI–CNT nanocomposites with different composition of CNTs in PANI were studied using SEM. Figure 1a represents the SEM image of pure PANI. The morphology of pure PANI exhibits a pattern in which the grains are bunched up, representing a granulated morphology, which is the most standard morphology in cases of PANI prepared by the chemical oxidation method. Figure 1b represents the SEM image of 5 wt.% of PANI–CNT nanocomposite. The composite synthesized by the in situ method are highly combined, and the morphology reveals that the CNT particles are mixed well in PANI matrix, and the grains are evidently distinguishable as tiny tubular structures with tube widths of 31.51 nm. However, the morphology of PANI–CNT nanocomposites entirely transformed into miniature tubes for the next 10 wt.% composite with the diameter of the CNTs about 31.49 nm. Also the tubular erections of CNTs specify the distribution of CNTs in PANI, as in Fig. 1c. With further rise in weight percentage of CNTs to 15 wt.%, a transition from a sphere shape to a tubular

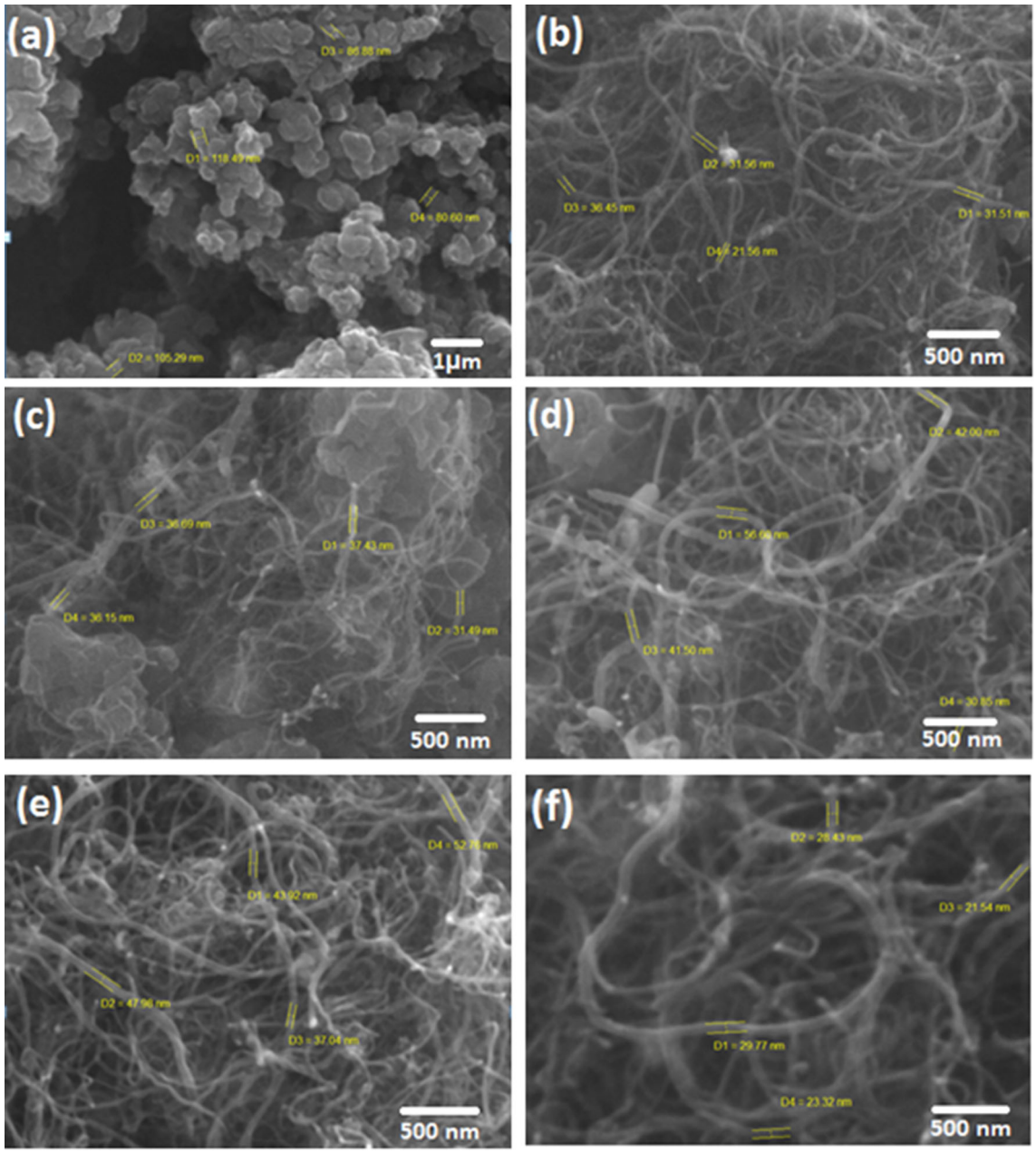

Fig. 1. SEM micrograph of (a) pure PANI, (b) PANI doped with 5 wt.% CNTs, (c) PANI doped with 10 wt.% CNTs, (d) PANI doped with 15 wt.% CNTs, (e) PANI doped with 20 wt.% CNTs, and (f) PANI doped with 25 wt.% CNTs.

morphology with the thickness of the tubes being 41.50 nm was observed. The formation of tiny rod-shaped layers increased in the composite structure with further rise in inclusion concentration of CNTs. The SEM images of CNT-doped PANI nanocomposite shown in Fig. 1d and e correspond to 20 wt.% and 25 wt.% composition, respectively, exhibiting a tiny tube-like structure with tube width of 37.04 nm and 29.74 nm. Thus, the SEM images confirm the formation of CNT-doped PANI after undergoing in situ polymerization.

FTIR

The FTIR spectra of pure PANI and PANI–CNT nanocomposites are depicted in Fig. 2. For PANI, the characteristic peak at 1635 cm^{-1} is assigned to C=C stretching vibration in the quinoid ring, and the peaks at 1527 cm^{-1} and 1517 cm^{-1} are assigned to stretching vibrations of C=C and C=N stretching in the benzenoid ring, respectively. The peak detected at 1485 cm^{-1} corresponds to C–C stretching vibrations in the aniline ring. The peaks at

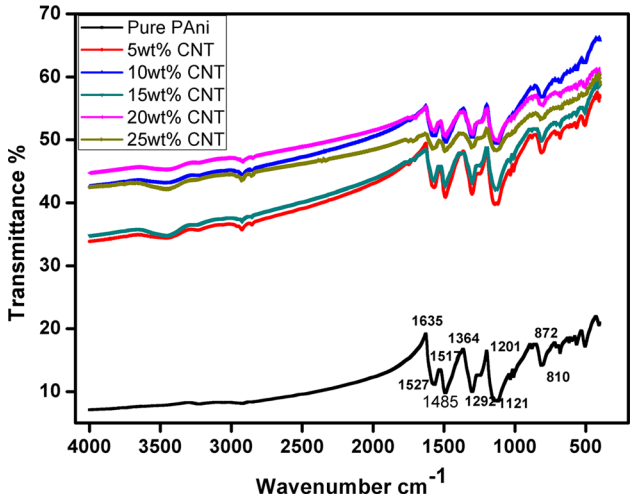

Fig. 2. FTIR spectrum of PANI and PANI–CNT nanocomposites.

1364–1292 cm^{-1} are attributed to a C–H in-plane deformation mode. The peaks originating between 872 cm^{-1} and 810 cm^{-1} can be interpreted as due to out-of-plane C–H bending vibration mode. Similarities were observed in the FTIR spectrum of PANI–CNT composite samples with a very slight shift in the position, and minute variation in the intensities of the peaks corresponding to PANI, thereby confirming the formation of the composites due to synergistic interaction between CNTs and PANI chains.[28]

Raman Spectroscopy

Raman spectroscopy is one of the important characterization techniques in material research, specifically in carbonaceous composites.[29] Figure 3 depicts the Raman spectra of pure PANI and its nanocomposites with CNTs. The Raman spectrum of pure PANI revealed two important characteristic peaks: D band (1347 cm^{-1}) and G band (1582 cm^{-1}). These bands are observed in the Raman spectrum of all the CNT-doped PANI composite samples. The D band is associated with the existence of edges and defects present in the sp^2 lattice representing pure CNT, and the G band is related to an sp^2 carbon network dispersed throughout the polymer matrix.[30,31] The pure PANI exhibits a peak at 2661 cm^{-1}, and CNTs exhibit the G band at 1576 cm^{-1} due to the Raman-active E_{2g} mode analogous in pure PANI, while the peaks at 1354 cm^{-1} (D band) and 2643 cm^{-1} (2D band) are generated from the defects in CNTs. The enhancement in the intensity of the D and 2D bands of CNTs after acid functionalization shows the connection of different functional groups over the surface of CNTs. Similarly, the peaks at 2000 cm^{-1}, 2100 cm^{-1}, and 2200 cm^{-1} are observed in the nanocomposites of higher weight percentages, while other peaks at lower concentrations are not apparent because they are too weak or are overlaid. The contribution and overlaying of peaks on one another

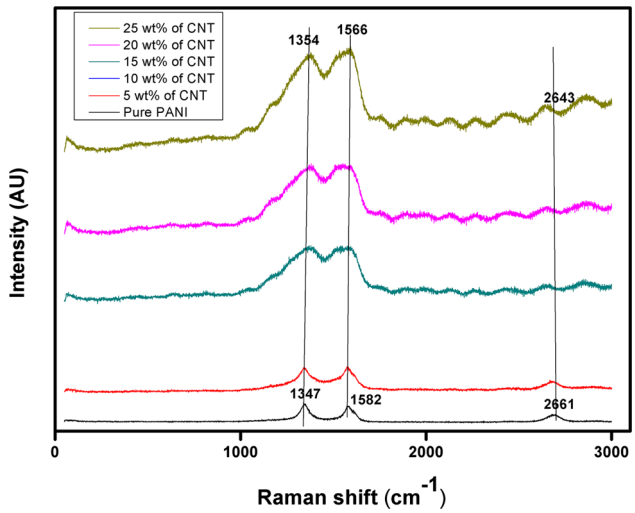

Fig. 3. Raman spectroscopy of PANI and PANI/CNT nanocomposites.

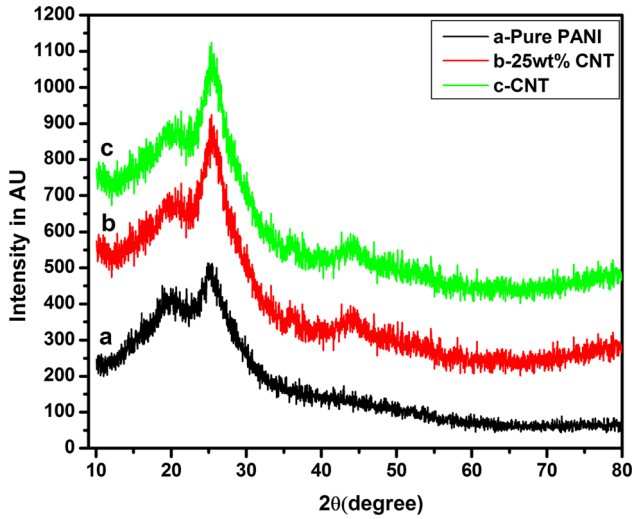

Fig. 4. XRD patterns of PANI and PANI/CNT nanocomposites.

(1354 cm^{-1}, 1576 cm^{-1}, and 2643 cm^{-1}) from the CNTs appear in PANI–CNT nanocomposites, giving rise to broad D and G Raman bands situated at 1354 and 1576 cm^{-1}, and their intensity was observed to increase with increasing CNT concentration. The interaction between the polymer matrix and CNTs with increasing weight percentages was elaborated and fitted with five Lorentzian curves. The band at 1582 cm^{-1} is attributed to the C=C stretching vibration in the quinonoid ring which is slightly shifted to 1576 cm^{-1} in the composite. However, the peaks at 1576 cm^{-1} and 1354 cm^{-1} are attributed to pure PANI and PANI–CNT nanocomposites. Thus, by employing the Raman spectroscopy technique, the molecular constituents and the nature of the bonds among them have been examined in detail.

XRD

The XRD patterns of PANI, CNTs and CNT-doped PANI nanocomposites are shown in Fig. 4a, b, and c. The XRD spectra of pure PANI (a) shows a broad reflection between $2\theta = 20°–30°$, which is a characteristic semi-crystalline peak of PANI synthesized by chemical oxidative polymerization.[32–34] The XRD spectra of pure CNTs (c) exhibit a broad peak centered around $\sim 2\theta = 28°$ which arises due to contributions from amorphous carbon of CNTs.[35,36] However, in the XRD patterns of PANI–CNT nanocomposites (b), the characteristic diffraction peak of PANI was influenced by the presence of CNTs. XRD spectra of the nanocomposite shows the presence of characteristic peaks corresponding to both PANI ($2\theta = 20°–30°$) and CNTs ($\sim 2\theta = 28°$, $\sim 2\theta = 45°$). These results clearly indicate that CNTs were well dispersed during in situ polymerization, resulting in nanocomposite formation.

Transport Properties

The aggregate involvement of electrical conductivity in conducting polymers is separated into a temperature-independent DC part and frequency-dependent AC part. The two-probe method and four-probe method are the most widely used techniques to measure the electrical parameters of the materials. The conductivities of pristine PANI and its nanocomposites with CNTs at 5 wt.%, 10 wt.%, 15 wt.%, 20 wt.%, and 25 wt.% ratios were determined using a laboratory-made setup consisting of a Keithley 2182, a nano-voltmeter, and a Keithley 6221 ammeter. The changes in DC conductivity with respect to temperature for all the samples are shown in Fig. 5. The DC conductivity values of all the samples remain almost constant up to a temperature of 110°C, and a substantial rise in values has been observed with increase in temperature. This phenomenon is attributed to thermally stimulated hopping of charge carriers, which is in accordance with the 1 D "Variable Range Hopping" model for disordered materials. Amongst all the composites, the conductivity values noted were highest for 10 wt.% of CNTs in PANI (0.53935 S/cm) which is about 5 times more than that of pure PANI. The fall in conductivity for the greater weight percentage samples can be attributed to the drop in the mobility of charge carriers with increasing filler content.

Figure 6 shows the change in frequency-dependent conductivity of CNT-doped PANI nanocomposites with respect to frequency. It is noticed that in the lower-frequency region, there is no specific variation in the conductivity up to a frequency of 10^6 Hz for all prepared samples including pure PANI. With further increase in the frequency above this range, the conductivity was observed to increase, which is a peculiar behavior of disordered systems and is in accordance with the universal power law.[37] Among all the samples, 10 wt.% of CNTs in PANI exhibits high conductivity (0.395 S/cm) which is about 7.5 times greater than that of pure PANI, as can be seen in Fig. 7. The enhancement in conductivity values due to frequency supports the polaron hopping mechanism. The reduction in conductivity for other samples might be because of disorderliness in the prepared composite with higher loading of CNTs.

Figures 8 and 9 represent the change in the real and imaginary (ε' and ε'') parts of the dielectric constant of CNT-doped PANI nanocomposites, respectively. The permittivity curves exhibit strong dispersion towards the lower-frequency range which remains unvaried with frequency beyond 10^3 Hz. The permittivity trend depicted in the plots is because of the interfacial polarization mechanism occurring in these composite materials.[38] Larger permittivity values at the low-frequency side are due to accumulation of a better percentage of charge carriers at the edge of the grain boundaries which participate in the polarization mechanism. At high

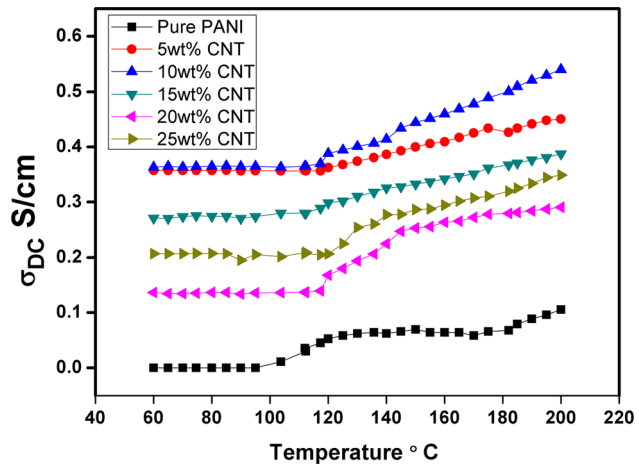

Fig. 5. Variations of temperature-dependent conductivity in PANI and PANI/CNT nanocomposites.

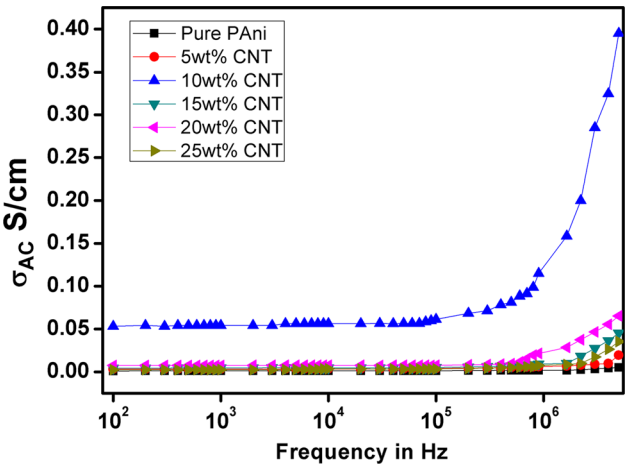

Fig. 6. Variations of frequency-dependent conductivity in PANI and PANI/CNT nanocomposites.

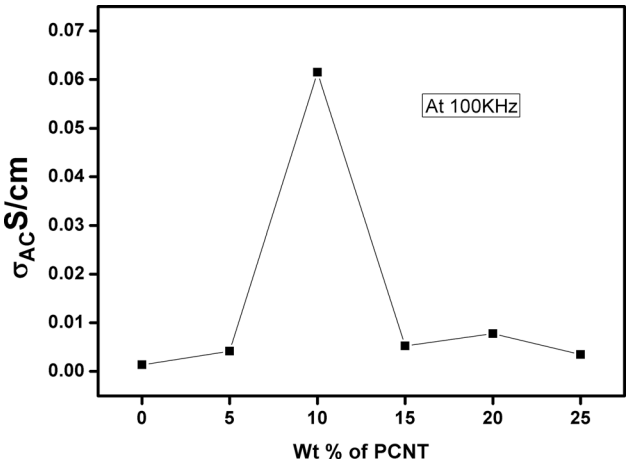

Fig. 7. Variations of frequency-dependent conductivity of PANI and PANI/CNT nanocomposites at 100 kHz.

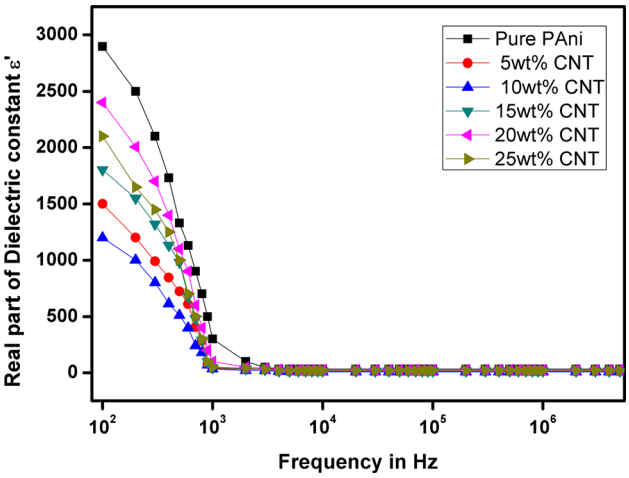

Fig. 8. Variations of the real part of the dielectric constant with respect to frequency of PANI at different concentrations of CNT nanocomposites.

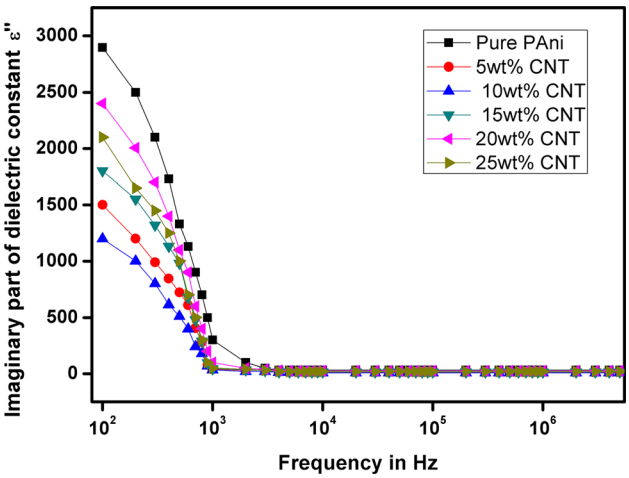

Fig. 9. Variations of the imaginary part of the dielectric constant with respect to frequency of PANI at different concentrations of CNT nanocomposites.

frequencies, the contribution of charge accumulation is minimal because the interaction between chains of PANI and CNT particles hinders the movement of the dipoles on account of which charge carriers fail to respond to the external field, and, hence, the dielectric constant value decreases. Among all the composite samples, it has been observed that the dielectric constant is low for the intermediate composite sample which is 10 wt.% of CNTs in PANI, and the values are about 3.5 times lesser than pure PANI.

The difference in the real part and the imaginary parts (Z' and Z'') of impedance with frequency for various wt.% of CNT-doped PANI nanocomposites are illustrated in Figs. 10 and 11, respectively. It can be noted that the values of both real and imaginary parts of impedance drops at greater frequencies, and the variations in the value of Z are found to depend on the loading concentrations of CNTs in the composites. Within the calibrated frequency scale for these samples, it is expected that different processes involving the space charge formation, dipole re-orientation, long-range mobility, or charge displacement over short distances might be the cause for impedance properties of the composite material. The occurrence of relaxation peaks in both Z' and Z'' might be because of the space-charge polarization mechanism. Thus, the conductivity increases appreciably with drop in impedance[39] for the 10 wt.% sample indicating that there is an effect of CNT particles at percolation in generating free charge carriers, and transformation of these charge carriers from one island to another is easier because of the fine grain boundary.

Figure 12 shows the Cole–Cole plot of PANI and CNT-doped PANI nanocomposites. It is observed that there is a significant drop in resistance with increase in both filler concentration and frequency. Bulk resistance and grain resistance are the two

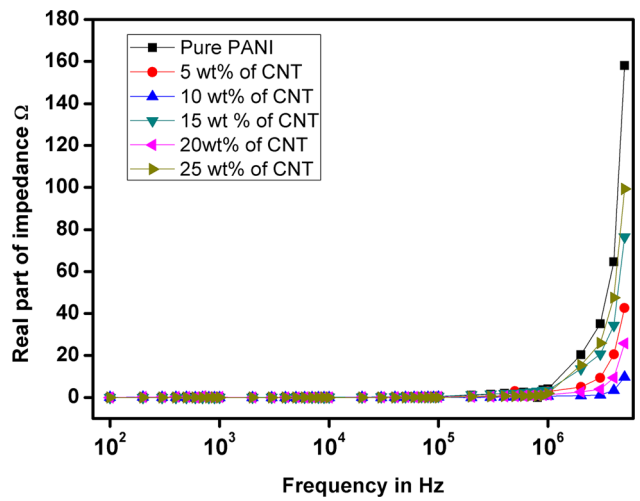

Fig. 10. Variations of the real part of impedance with respect to the frequency of PANI at different concentrations of CNT nanocomposites.

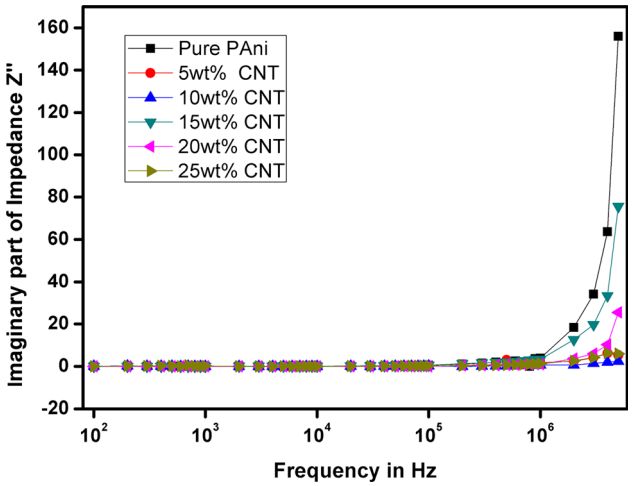

Fig. 11. Variations of the imaginary part of impedance with respect to the frequency of PANI at different concentrations of CNT nanocomposites.

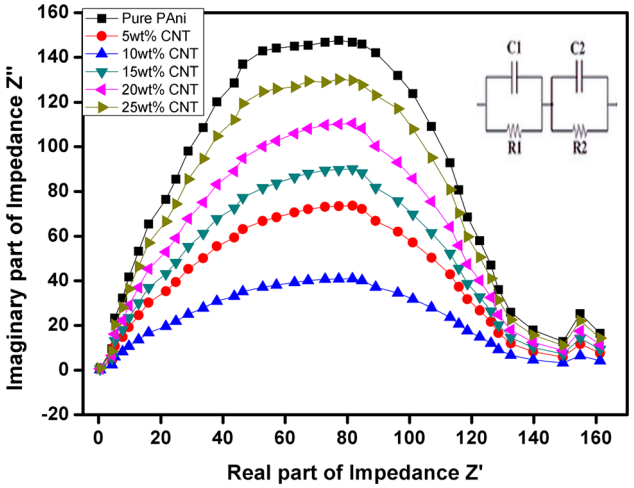

Fig. 12. Cole–Cole plot of PANI and PANI/CNT nanocomposites.

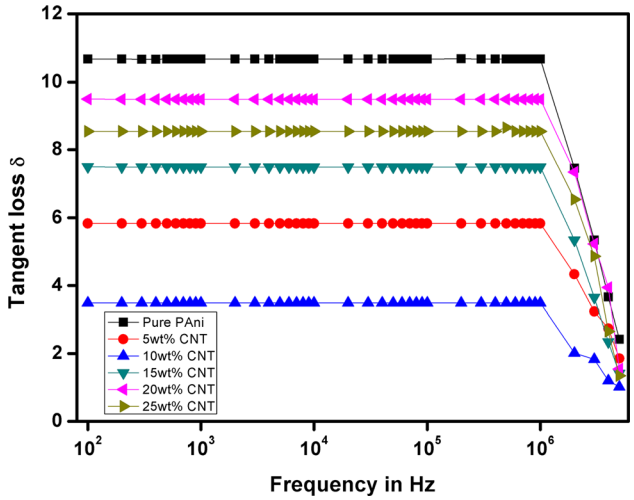

Fig. 13. Variation of tangent loss of PANI and PANI/CNT nanocomposites.

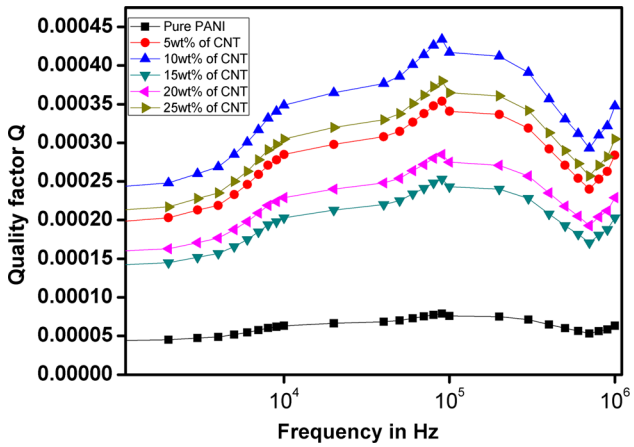

Fig. 14. Variation of quality factor of PANI and PANI/CNT nanocomposites.

factors in a complex inductor/resistor/capacitor (LCR) circuit on which the impedance values depend. The bulk and grain resistances drop with rise in CNT concentration which in turn results in the drop of impedance values.[40,41] It is observed that as loading percentage increases, the area below the curve decreases up to the percolation threshold, indicating a sharp drop in resistance. The semicircular arcs specify the existence of two variable constituents in the composite which can be regarded as a combination of series resistor and the geometrical capacitance. The arc area gradually decreases with increase of concentration of CNTs in PANI, indicating a sudden increase of the conductivity of CNT-doped PANI nanocomposites. In the Cole–Cole plots of pure PANI and CNT-doped PANI composites, the two peaks observed indicate the presence of different components in the composites contributing to the resistance. Of the samples, the 10 wt.% composite exhibits small bulk resistance as time taken for relaxation is very low compared to other samples.

Figure 13 represents the variation in tangent loss for PANI and CNT-doped PANI nanocomposites. The concept of dielectric loss can be explained based on the phenomenon of relaxation which can be of three types: dipole relaxation losses, deformational losses, and conduction losses.[42] It can be seen in the plot that the loss factor tan δ was almost constant in all the samples and dropped toward the higher-frequency region. The energy losses are noticed to be very small beyond 10^5 Hz. With further rise in the frequency up to 10^6 Hz, the dielectric loss is found to drop significantly, indicating an easy charge transfer from one end to the other end of the polymer chains.[43] Among all the composites, the 10 wt.% composite exhibits low dielectric loss compared to pure PANI. The losses are minimal beyond 10^6 Hz, indicating these composites behave as lossless materials in the high-frequency range.[44]

Figure 14 represents the variation of quality factor (Q) with the frequency for different loading of CNT-doped PANI nanocomposites. Here, it is noticed that there is a significant change in the values of the quality factor with varying concentration of CNTs and also with frequency. It is observed that the quality factor value is constant initially for all the prepared composites. However, all the composites exhibited a broad maxima spread in the mid-frequency range between 10^4 Hz and 10^5 Hz, out of which the 10 wt.% composite exhibits 5.5 times improved values of the quality factor compared to that of pure PANI.

Corrosion Studies

Corrosion or erosion is a destructive phenomenon induced either chemically or electrochemically that can be incurred to any alloys or metal surface via chemical reaction within the existing environment and, in some extreme cases, causes failure in the structure of the materials. The films or coatings are prepared in order to avoid the corrosion due to various reasons. Such types of coatings are otherwise called as inhibitors. Based on the various parameters, they are classified as mentioned below.

Inhibitor Classification

Corrosion inhibitors are chemical substances which can be available either in synthetic or natural form. These inhibitors are classified as follows: the first one is an organic or inorganic form of chemical, the second one is the reaction mechanism either as an anodic or cathodic mix or, in some cases, both as absorptive action, and the third one is as an oxidizing chemical. The inorganic material inhibitors show either cathodic or anodic actions. The organic inhibitors exhibit both cathodic and anodic actions and acts as a corrosion protective layer in the form of film over the metal surface.

The present study is carried on using organic inhibitors, which are made up of pure PANI and PANI–CNT films prepared by dip-coating method. The proficiency of an organic inhibitor is based on the chemical structure, molecular size of the organic compound, aromaticity, and conjugated bond length in carbon and other types of solution which can be easily soluble in the environment.

Corrosion Protection Efficiency Measurements

The 316L stainless-steel substrates of an area (2 cm × 2 cm) coated with various concentrations of PANI–CNTs are placed in 1 molar HCl. The pure PANI and PANI–CNT nanocomposites are characterized in 1 molar HCl through Tafel polarization curves, as depicted in Fig. 15. The rectilinear parts of the recorded Tafel curves are extrapolated to get the current density in the corrosion media (I_{corr}), corrosion potential (E_{corr}), and anodic and cathodic

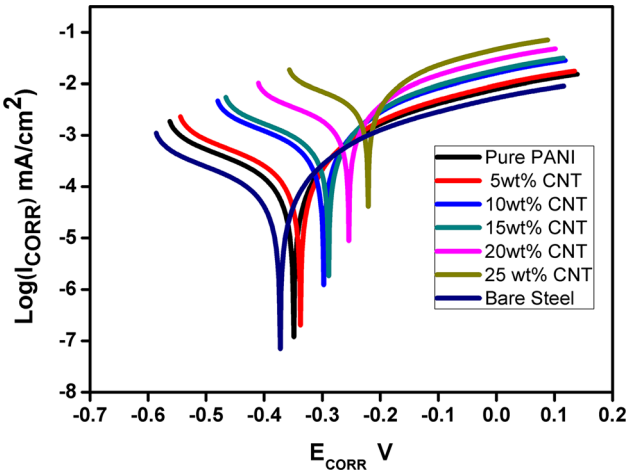

Fig. 15. Tafel plots with respect to the potential of PANI and PANI/CNT nano composites.

Tafel constants (β_a, β_c or b_a or b_c). Generally, in the open-circuit potential, the anodic sweep in the range of ± 0.200 V is applied to perform the Tafel measurement in 1 molar HCl at the scan rate of 1 mV/S. Before Tafel measurements, the pure PANI and PANI–CNT nanocomposites were immersed in 1 molar HCl solution till stable, and constant values were obtained for the E_{OCP}. For calculating the corrosion rate parameters automatically, Ivium Soft software (version 1.832) was employed. The electrochemical impedance spectroscopy (EIS) experiments were carried out at E_{OCP} for different substrates at varying immersion times such as 4 h, 8 h, 12 h, 16 h, and 20 h in 1 molar HCl solution. Also, the amplitude was set for 5 mV, and frequency was varied in the range of 10^5–0.1 Hz.

The improvement of anticorrosion properties in composite films of PANI doped with CNTs may be due to well-dispersed CNTs in PANI matrix that enhances the diffusion pathways for oxygen and water vapors. The detailed corrosion mechanism and creation of rust on a mild steel substrate, which involves many steps such as reduction and oxidation, can be illustrated through the following reactions.[45]

$$Fe \rightarrow Fe^{2+} + 2e^- \quad (1)$$

$$Fe^{2+} \rightarrow Fe^{3+} + 1e^- \quad (2)$$

$$O_2\,(gas) + 2H_2O + 4e^- \rightarrow 4OH^- \quad (3)$$

$$2Fe^{2+}\,(aq) + O_2\,(gas) + 2H_2O \rightarrow 2FeOOH + 2H^+ \quad (4)$$

From the above equations, it can be inferred that there is enough requirement of water and oxygen for the creation of rust and dissolution of the steel, leading to corrosion. So, by controlling any of these

Table I. Polarization parameters of PANI and PANI–CNTs

Sample no.	Details of composites	E_{corr} (mV)	I_{corr} (mA/cm^2)	b_a (mV/dec)	b_c (mV/dec)
1	Pure PANI	−345	6.98	85	112
2	PANI–5 wt.%CNT	−333	6.85	80	101
3	PANI–10 wt.%CNT	−296	5.89	74	96
4	PANI–15 wt.% CNT	−278	5.63	69	87
5	PANI–20 wt.% CNT	−249	5.03	63	79
6	PANI–25 wt.% CNT	−219	4.38	57	71

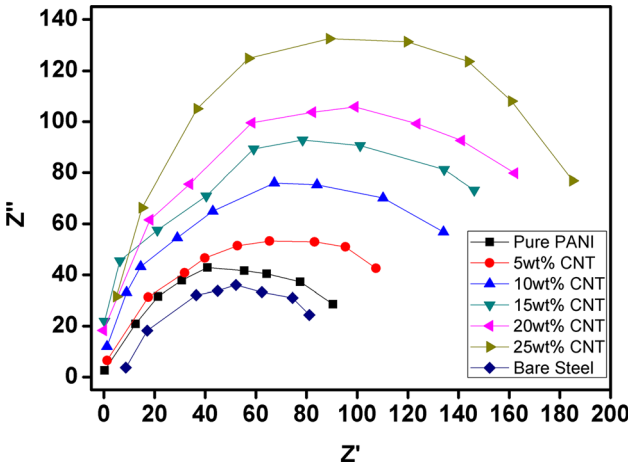

Fig. 16. Nyquist plots of PANI and PANI/CNT nanocomposites.

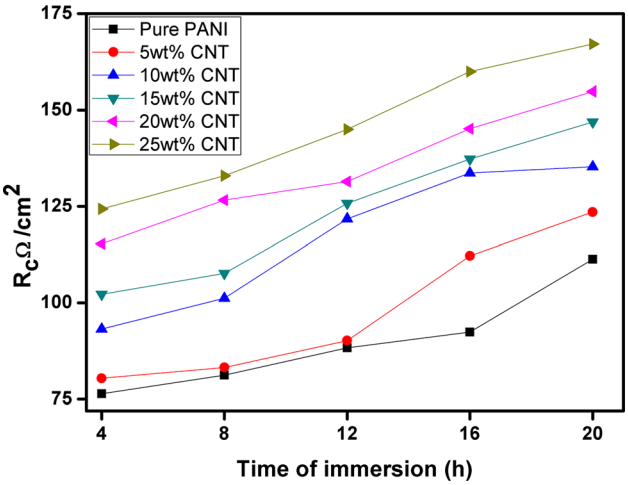

Fig. 17. Variation of time with resistance of PANI and PANI–CNT nanocomposites.

chemical reactions, the corrosion process gets inhibited, and thereby the coating surface becomes more effective for corrosion control. Therefore, it is believed that the enhancement of the diffusion pathways in the polymer matrix significantly prevents water and oxygen on the steel substrates, thereby exhibiting good anticorrosion properties.

Table I represents the polarization parameters for pure PANI and its nanocomposites with CNTs. The I_{corr} values may be affected by the steel substrate corrosion and by the redox chemical reaction of electrically active polymer films.[46] The results obtained confirmed that the corrosion current alters the current density.[47]

The iron metal dissolved in the acidic media at the time of anodic reaction signifies that the electrons are ejected from the metal, resulting in both oxygen and hydrogen species getting easily dissolved in the solution. At the earlier stage, the cathodic chemical reaction occurs over the metal surface, and then it is transferred to the polymer electrolyte blend. This behavior might be due to conducting characteristics of electrically active polymers.[48] Thus, for different loadings of dopant in host polymer matrix, the E_{corr} significantly changes. The results revealed that the 316L stainless steel coated with PANI–CNTs (25 wt.%) exhibited a maximum transfer when the potential of the cathode was 0.345 V. The two main reasons for the major transfer are probably the inclusion of anions into host polymer and the electrically active coating of conducting polymer.

Electrochemical Impedance Spectroscopy Measurements

In the process of investigating anticorrosion properties, an impedance measurement is a broadly used tool. It provides essential knowledge of both the capacitance and the resistance behavior at the interface region and facilitates the exact assessment of performance in the inhibitor composites. Figure 16 indicates the impedance spectra (Nyquist plot) recorded for 316L stainless-steel substrate dipped in 1 molar HCl solution at room temperature in the presence of different inhibitor concentrations. It is observed that in the Nyquist plot, the area under the curve decreases with increase of CNTs in PANI, and this behavior clearly implies a drop in the grain and bulk resistance in the composites.

By loading different concentrations of inhibitor in PANI–CNT nanocomposites, a change in the electrical resistance has been observed, as depicted in Fig. 17. Each individual concentration of the inhibitor has a semicircular graph. The area under each curve could be connected to the degree of the corrosion rate. The area under the curve varies when loaded with different inhibitor concentrations,

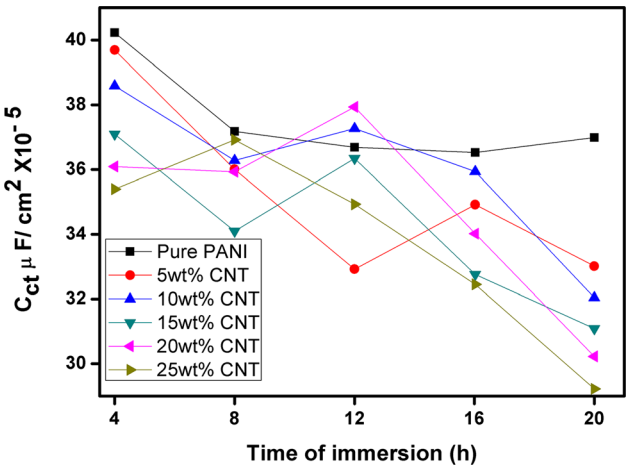

Fig. 18. Variation of time with capacitance of PANI and PANI–CNT nanocomposites.

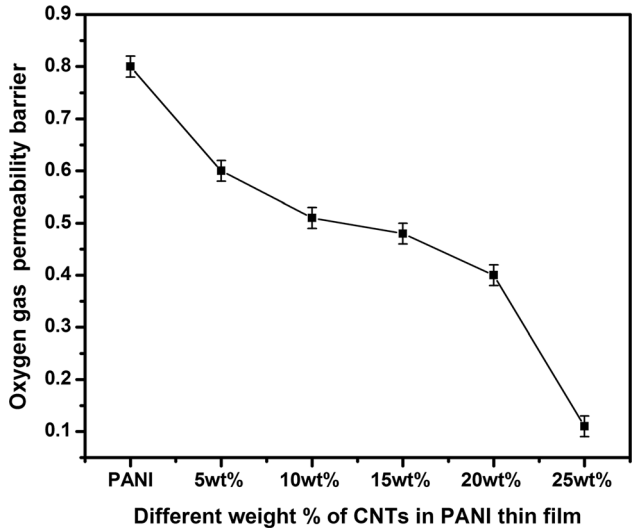

Fig. 19. Oxygen gas permeability of PANI and PANI–CNT nanocomposites.

indicating a significant drop of the corrosion rate, which translates into an improvement in the anti-corrosion rate. The semicircular graph in Fig. 17 is not perfect due to increase in the concentration of inhibitor in the corrosive solution and also due to the surface roughness and some imperfections over the surface of 316L steel substrate. This anomaly is known as "dispersing effect" and this can also be interpreted upon analysis that a slow corroding system may be the result of a large resistance during charge transfer.[49]

In EIS studies, Gamry Echem Analyst software is used to analyze charge transfer parameters of resistance (R_{ct}), and the double-layer charge capacitance. Figures 18 and 19 reveal increased R_c values, and C_{dl} values were reverse in PANI and its nanocomposites. The increase in R_c values shows that a firm passive layer has been formed at the interface of polymer and electrode so that corrosion inhibition can be effective. A decrease in the values of C_{ct} is observed with increased time of immersion. This may be due to the formation of dense layers of CNTs in the polymer matrix at the interface of the electrode, which supports a maximum resistance and, therefore, can be considered as an effective anticorrosion protection. Because of the high resistance being developed, charge accumulation reduces; in other words, capacitance will reduce. The value of the resistance was observed to be maximum for 25 wt.% PANI–CNT coating. The present study reveals that PANI doped with 25 wt.% of CNTs possesses higher anticorrosion properties, this behavior is mainly due to formation of more charges (polarons/bipolarons) in the polymer matrix upon doping which easily facilitate charge carriers in the backbone and anticorrosion behavior in this composite.

In this study, the investigations have revealed that PANI composite film doped with 25 wt.% of CNTs has good corrosion protection properties in comparison with pure PANI film. The thin films of the composite materials prepared herein displayed a larger gas barrier. Doping of PANI with CNTs has resulted in the creation of a good number of conducting pathways, and these pathways affect the gas molecules by retarding the molecular mechanism within the polymer chain.[50,51] The effect of this has resulted in a decrease of the permeability values and improvement in the corrosion protection properties of the samples. Among all the samples, PANI composite film doped with 25 wt.% of CNTs is realized to have more conducting pathways which in turn are associated with greater reduction in the values of oxygen gas permeability compared to that of pure PANI film. Therefore, the composite film with 25 wt.% of CNTs in PANI is regarded to be as percolation threshold having a better gas barrier than pure PANI film.

From the Fig. 19, it is clear that the composite film with 25 wt.% of CNT doped in PANI shows better gas barrier property in comparison to pure PANI film. The reduction of oxygen permeability is approximately 66%, and this could be attributed to the higher aspect ratio of the composite film at the percolation threshold. The gas permeability studies have revealed that PANI films doped with CNTs are more suitable as advanced gas-barrier materials for anticorrosion. Therefore, these composite films of PANI doped with CNTs have gained huge potential to replace conventional anticorrosion materials.

CONCLUSION

In the present work, CNT-doped PANI nanocomposite pellets and thin films were successfully synthesized via in situ polymerization and dip-coating methods, respectively. The prepared composites were characterized by FTIR, XRD, SEM, and micro-Raman spectroscopy techniques, which have provided a handful of information about the structure of the material, degree of crystallinity,

morphology, composition, and specific interactions between the molecules. CNTs are compatible with polyaniline matrix when added to it, the combination of which has led to significant changes in electrical properties due to synergistic interaction between them. The increased interchain and conformational changes lead to enhancement of conductivity as observed through AC and DC conductivity results. Among the CNT-doped PANI nanocomposites, the 10 wt.% composite exhibits the maximum value of conductivity due to increase in conjugation length and also due to thermally stimulated hopping of charge carriers. The conductivity reduces for other wt.% samples, which is an indication that the percolation behavior is being observed in these composite systems at a percolation threshold of 10 wt.% of CNTs in PANI. Also the addition of CNTs as filler in PANI has greater influence on dielectric parameters such as the dielectric constant and dielectric loss. In corrosion studies, the 25 wt.% of PANI–CNTs sample offers high resistance to the corrosion due to the formation of dense multilayered chains of CNTs. The 25 wt.% of PANI–CNT coating on mild steel was determined to be effective for protection against corrosion and is indicative that it protects the steel due to the better oxygen barrier. These material composites can be used for most of the modern optoelectronic devices and also as the corrosion protection materials for future technology.

ACKNOWLEDGMENTS

The authors would like to thank the management and Principal of PES University, Bangalore South Campus, for their cooperation and assistance to carry out this research work.

REFERENCES

1. A.S. Curran and M.P. Ajayan, *Adv. Mater.* 10, 1091 (1998).
2. M. Cochet and W.K. Master, *Chem. Commun.* 10, 1450 (2001).
3. H. Zengin and W. Zhou, *J. Adv. Mater.* 14, 1480 (2002).
4. P.M. Ajayan and O. Stephen, *J. Sci.* 265, 1212 (1994).
5. P.M. Ajayan, *Chem. Rev.* 99, 1787 (1999).
6. H.R. Baughaman and A.A. Zakhidov, *J. Sci.* 297, 787 (2002).
7. T.E. Thostenson and Z. Ren, *Sci. Technol.* 61, 1899 (2001).
8. M. Moniruzzaman and K.I. Winey, *Macromolecules* 39, 5194 (2006).
9. E. Kymakis, *Appl. Phys. Lett.* 80, 112 (2002).
10. J. Michael and O. Connell, *Chem. Phys. Lett.* 342, 265 (2001).
11. G. Mittal, V. Dhand, K.Y. Rhee, S.J. Park, and W.R. Lee, *J. Ind. Eng. Chem.* 21, 11 (2015).
12. S. Palaniappan and A. John, *Prog. Polym. Sci.* 33, 732 (2008).
13. W.K. Jang, J. Yun, H.I. Kim, and Y.S. Lee, *J. Carbon Lett.* 12, 162 (2011).
14. J. Yun, H.I. Kim, and Y.S. Lee, *Appl. Surf. Sci.* 258, 3462 (2012).
15. T.H. Le, N.T. Trinh, L.H. Nguyen, H.B. Nguyen, V.A. Nguyen, and T.D. Nguyen, *Adv. Nat. Sci. Nanosci. Nanotechnol.* 4, 025014 (2013).
16. M.S. Dorraji, I. Ahadzadeh, M.H. Rasoulifard, and M. Chitosan, *Int. J. Hydrog. Energy* 39, 9350 (2014).
17. H. Zhang, B. He, Q. Tang, and L. Yu, *J. Power Sources* 275, 489 (2015).
18. H.F. Cui, L. Du, P.B. Guo, and B. Zhu, *J. Power Sources* 283, 46 (2015).
19. A.M. Kumar and Z.M. Gasem, *Prog. Org. Coat.* 78, 387 (2015).
20. R. Kumar, H.K. Choudhary, S.P. Pawar, S. Bose, and B. Sahoo, *Phys. Chem. Chem. Phys.* 19, 23268 (2017).
21. M. Wu, Y.W. Lin, and C.S. Liao, *Carbon* 43, 734 (2005).
22. J.A. Syed, H. Lu, S. Tang, and X. Meng, *Appl. Surf. Sci.* 325, 160 (2015).
23. Y. Chen, X.H. Wang, J. Li, J.L. Lu, and F.S. Wang, *Corros. Sci.* 49, 3052 (2007).
24. D.P. Le, Y.H. Yoo, J.G. Kim, S.M. Cho, and Y.K. Son, *Corros. Sci.* 51, 330 (2009).
25. C.-H. Chang and T.-C. Yeh, *Carbon* 50, 044 (2012).
26. Z.H. Zhang, D.Q. Zhang, L.H. Zhu, L.X. Gao, T. Lin, and W.G. Li, *J. Coat. Technol. Res.* 14, 1083 (2017).
27. M. Lakshmi, A.S. Roy, and S. Khasim, *AIP Adv.* 3, 112 (2013).
28. G. Theivandran, M. Ibrahim, and S. Murugan, *J. Med. Plants Stud.* 3, 30 (2015).
29. A.C. Ferrari and J. Robertson, *J. RSC* 362, 1824 (2004).
30. A. Eckmann, A. Felten, I. Verzhbitskiy, R. Davey, and C. Casiraghi, *Phys. Rev. B* 88, 035426 (2013).
31. F. Tuinstra and J.L. Koenig, *J. Chem. Phys.* 53, 1126 (2003).
32. T.M. Wu and Y.W. Lin, *Polymer* 47, 3576 (2006).
33. S. Khasim, *Results Phys.* 12, 1073 (2019).
34. S. Khasim and M. Lakshmi, *Polym. Compos.* 10, 24895 (2018).
35. R. Kumar, A. Kumar, N. Verma, A.V. Anupama, R. Philip, and B. Sahoo, *Carbon* 153, 545 (2019).
36. R. Kumar, R. Rajendiran, H.K. Choudhary, G.M. Naveen Kumar, B. Balaiah, A.V. Anupama, and B. Sahoo, *Nano-Struct. Nano-Objects* 12, 229 (2017).
37. P. Kar and A. Choudhury, *Sens. Actuators B Chem.* 183, 25 (2013).
38. J.C. Dyre Schroder, *Rev. Mod. Phys.* 72, 873 (2000).
39. S. Khasim and O.A. Al-Hartomy, *RSC Adv.* 4, 39844 (2018).
40. A. Mishra and S.N. Choudhary, *Phys. B* 406, 3279 (2011).
41. Z.D. Xiang, T. Chen, and X.C. Bian, *Macromol. Mater. Eng.* 294, 91 (2009).
42. K. Wakabayashi, M. Fujita, H. Ajiki, and M. Sigrist, *Phys. B* 280, 388 (2000).
43. A. Kyritsis, P. Pissis, and J. Grammatikakis, *J. Polym. Sci. Part B Polym. Phys.* 33, 1737 (1995).
44. A.O. Al-Hartomy, S. Khasim, A. Roy, and A. Pasha, *Appl. Phys. A* 125, 12 (2019).
45. L.N. Shubha and P. Madhusudhan Rao, *Int. J. Sci. Eng. Res.* 6, 11 (2015).
46. W.S. Tait, Docs Publications (1994), p. 57.
47. C.K. Tan and D.J. Blackwood, *Corros. Sci.* 45, 545 (2003).
48. P. Ocon, A.B. Cristol, P. Herrasti, and E. Fatas, *Corros. Sci.* 47, 649 (2005).
49. S. Sathiyanarayanan, S. Muthukrishnan, and G. Venkatachari, *Prog. Org. Coat.* 64, 460 (2009).
50. K.F. Khaled, *Electrochim. Acta* 48, 2493 (2003).
51. D.W. De Berry, *J. Electrochem. Soc.* 132, 1022 (1985).